

# Variability in Fatigue Life of Near- $\alpha$ Titanium Alloy IMI 834

Litton Bhandari<sup>1</sup> · Jalaj Kumar<sup>2</sup>  · I. Balasundar<sup>2</sup> · Amit Arora<sup>1</sup>

Received: 28 September 2020 / Accepted: 31 January 2021 / Published online: 10 March 2021  
© The Indian Institute of Metals - IIM 2021

**Abstract** Most aero-engine components and structures are subjected to life critical fatigue loads during service. Near- $\alpha$  titanium alloy IMI 834 is one candidate aero-engine material that is used as high-pressure compressor discs due to its superior fatigue strength and creep resistance. The effect of heat treatment on the microstructure and high-cycle fatigue behaviour of the material has been studied and reported here. The alloy was solution-heat-treated at 1060 °C and subsequently quenched in different media. A strong effect of quench media (cooling rate) on high-cycle fatigue life has been observed. Fractographic investigations were performed to correlate the fracture micro-mechanism with heat treatment. Further, a generalized stress-life model has been deduced from the fatigue data and integrated with finite element analysis to develop a fatigue model for the alloy.

**Keywords** IMI 834 · Heat treatment · High-cycle fatigue · Stress-life model

## 1 Introduction

Titanium alloys are characterized by high strength, better toughness and better mechanical properties. Titanium has better corrosion-resistant properties and shows good heat-resistant properties [1–3]. Titanium alloys have been

extensively used for aero-engine components. IMI 834 is one of the competing candidates which have been developed to meet the demand of the aero-engine components such as better fatigue and creep performance at an elevated temperature. Most rotating aero-engine components are subjected to repeated loading and hence fail by fatigue. Earlier studies [4] indicate that the fatigue damage constitutes a major cause of failure of aero-engine components. Two types of fatigue, namely low-cycle fatigue (LCF) and high-cycle fatigue (HCF), are encountered in the aero-engine components. While thermal loads create LCF damage, aerodynamic-related excitations at natural frequencies lead to HCF damage. Hence, design against fatigue becomes one of the important issues in aero-engine component design. These fatigue properties are known to be dependent on the microstructure of the material. Microstructural features such as morphology, age-hardening conditions, grain size, work hardening, volume fraction, crystallographic texture, etc., strongly affect the fatigue behaviour of the titanium alloys [5, 6]. IMI 834 is a near-alpha titanium alloy which has been designed for improved fatigue performance and creep strength for application at a higher temperature. IMI 834 is relatively the recent titanium alloy in which carbon is added in small amount (0.06wt %) to widen the heat treatment window as compared to its predecessor IMI 829 [7, 8]. Carbon being the  $\alpha$ -stabilizer and strengthening element has another important role in widening the temperature range over which the transition from  $\alpha$  to  $\beta$  occurs. A wide range of microstructure can be generated by varying the solution heat treatment (SHT) temperature and cooling rate. Hence, the microstructure can be optimized with respect to the required properties.

Microstructure strongly influences the fatigue strength in titanium alloys. Wu et al. [9] and Ivanova et al. [10]

---

✉ Jalaj Kumar  
jalaj@dmrl.drdo.in

<sup>1</sup> Indian Institute of Technology Gandhinagar, Gandhinagar  
382355, India

<sup>2</sup> Defence Metallurgical Research Laboratory, Hyderabad  
500058, India

showed that the bimodal microstructure has higher fatigue strength as compared to equiaxed microstructure and lamellar microstructure. However, Zuo et al. [11] and Lutjering et al. [12] observed an opposite result. It has not been well explained about the contradictions in the results. In case of near- $\alpha$  Ti alloys and  $\alpha + \beta$  Ti alloys, the width of  $\alpha$  lamellae in the lamellar microstructure,  $\beta$  grain size in the equiaxed microstructure and the size of lamellae in duplex microstructure are the important microstructural parameters which affect the fatigue life [13]. It was also noted that the fatigue strength is highly affected by the grain size and primary  $\alpha$  content [9, 10, 14, 15]. Wu et al. [16] reported that the fatigue strength increases with the increase in the percentage of primary alpha in  $\alpha + \beta$  titanium alloys at room temperature. Furthermore, the high-temperature fatigue strength is comparable with increasing the percentage of primary alpha. A number of studies have been carried out on cyclic stress response of IMI 834 at elevated temperature, and the effect of temperature and environmental conditions has been investigated [17]. Hardt et al. [18] investigated the high-temperature fatigue damage mechanism in near- $\alpha$  titanium alloy IMI 834. Fatigue life is largely dependent on the maximum stress of the fatigue cycle at a lower temperature. However, the fatigue life at higher temperature is governed by the environmental degradation due to the formation of brittle oxygen-enriched subsurface. IMI 834 has better creep, fatigue and crack propagation properties in bimodal microstructure containing 15 vol% of primary  $\alpha$  embedded in the matrix of transformed  $\beta$  with lamellar structure [17]. The fatigue properties are also dependent on the surface conditions. The variability in fatigue life of  $\alpha + \beta$  titanium alloys at all stress levels is the same in case of low stress grinding (LSG) samples, whereas comparable scatter is observed in fatigue life of electro-polished (EP) specimen [19]. The LSG imparts controlled compressive residual stresses, whereas EP removes those residual stresses and imparts highly polished surface finish. Internal crack initiation under tensile mean stress condition results in lowering the fatigue strength as compared to surface and subsurface crack initiation [20]. The cleavage facets from the  $\alpha$  grains are considered to be the crack origin for titanium alloys during cyclic loadings [21].

Several investigations have been done to study the effect of heat treatment on the microstructure and monotonic behaviour of near- $\alpha$  titanium alloy as discussed above. But, a handful of data are available on the effect of various heat treatments on the fatigue behaviour as well as the numerical modelling and simulation associated with it. In the present study, an attempt has been made to bridge this gap. Variability in the microstructure of IMI 834 is generated by varying the heat treatment conditions, and studies have been done here to investigate the effect of heat treatment

conditions on the microstructure and fatigue behaviour of near- $\alpha$  titanium alloy IMI 834. Furthermore, numerical modelling and simulation have been done and extended to the component level to showcase the effect of heat treatment on life prediction.

## 2 Experimental Procedures

### 2.1 Materials

The elemental composition of the near- $\alpha$  titanium alloy IMI 834 is given in Table 1. The  $\beta$ -transus temperature of the indigenous material was reported to be 1060 °C.

### 2.2 Isothermal Forging

Billets of diameter 150 mm by 162 mm height were extracted from the as-received bar stock and coated with Deltaglaze 347 to prevent oxidation of the material. The coated material was heated to 925 °C in an electrical resistance heating furnace equipped with Kanthal heating elements. A soaking time of 180 min was provided in order to ensure thermal equilibrium in the material. The flat IN100 dies mounted on the forge press were heated to the required temperature of 910 °C using induction heaters. The billet was then transferred to the forge press using a robot pick-move car, and a deformation (height reduction) of 72% was imparted to the material with an equivalent strain rate of  $10^{-3}$ /sec. The deformed material was then removed from the forge press and cooled in air.

### 2.3 Heat Treatment

Samples were extracted from the as-received materials. These samples so extracted were heated in a box muffle furnace with a uniform heating zone of  $100 \times 100 \times 100$  mm<sup>3</sup> after coating with Deltaglaze 347®. These samples were soaked for 30 min after attaining thermal equilibrium. Solution heat treatment (SHT) of the isothermally forged samples was done at a temperature of 1060 °C. After allowing 2-h soaking time at a particular solution heat treatment temperature, samples were quenched in different cooling media (water, oil, air and furnace). All the samples were aged at  $700 \text{ °C} \pm 2 \text{ °C}$  for a duration of 2 h after solution heat treatment and cooled in ambient air (Table 2). Then, samples were extracted for high-cycle fatigue test. The cooling rate of the quenching media was evaluated as per to the ASTM D6200-01. A probe of 12.5 mm diameter and 66 mm height was extracted. A hole of 4 mm diameter was drilled into the probe, and K-type thermocouple was inserted. This thermocouple was connected to a chartless recorder which recorded the temperature at an interval of

**Table 1** Elemental composition of near- $\alpha$  titanium alloy IMI 834

Elements	Ti	Al	Sn	Zr	Nb	Mo	Si	C
wt%	85.19	5.8	4.0	3.5	0.7	0.5	0.25	0.06

**Table 2** Details of heat treatment conditions used for the present study

Soaking time	120 min			
Temperature	1060 °C			
Cooling medium	Furnace	Air	Oil	Water
Cooling rate (°C/min)	16	490	3620	8500

125 ms. The probe was then inserted into the quenching media whose cooling rate was to be evaluated.

#### 2.4 Microstructural and Hardness Examination

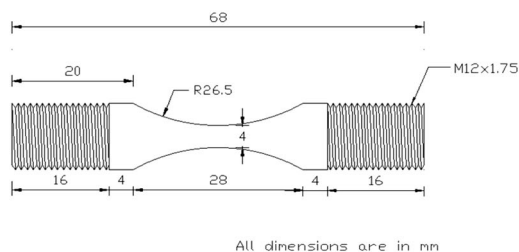
Both optical and scanning electron microscope (SEM) analyses were performed in the present study. The samples were cut using a precision cutting machine. The cut samples were mounted using hot moulding and polished till mirror-like surface finish was obtained. Kroll's reagent was used to investigate the required and desired microstructural features. The microstructures were examined, and microscopic images were taken using optical and scanning electron microscope. Important microstructural parameters were evaluated using Image J software and other stereological tools. A Buehler hardness test machine was used to evaluate the surface bulk hardness of the IMI 834. A right pyramidal diamond indenter was used and pressed onto the sample with a load of 20 Kgf. The dwell time was kept as 20 s.

#### 2.5 High-Cycle Fatigue Test

Hourglass-type specimens were used for high-cycle fatigue (HCF) test. Dimensions were decided as per the guidelines given in ASM handbook as shown in Fig. 1. Cylindrical

rods of 68 mm length and 12 mm diameter were extracted from various heat treated conditions. Hourglass specimens with a highly polished gauge section having a diameter of 4 mm were used. High-cycle fatigue (HCF) test is greatly affected by the surface roughness of the specimen. In order to avoid the scatter in the final data, special care was taken to prepare the sample. The samples were mechanically polished using successive finer grades of polishing papers ranging from 600- to 1200-grit waterproof silicon carbide paper. Diamond paste in the circumferential direction was used for the final polishing. This procedure enabled a mirror finish of the specimen.

The specimens after polishing were tested on a computer-controlled servo-hydraulic testing machine (Model: BISS). The operating frequency was kept in between 10 and 20 Hz. The test monitored load levels, frequency and cycle numbers. Further, fractured surfaces were extracted from the fractured specimen and thoroughly cleaned ultrasonically with acetone. The surfaces of the fractured samples were examined using scanning electron microscope (SEM) to identify the fracture modes and micro-mechanism of high-cycle fatigue (HCF).

**Fig. 1** High-cycle fatigue specimen

### 3 Results and Discussion

#### 3.1 Effect of Heat Treatment on Microstructure

The microstructure of heat-treated IMI 834 alloy consists of colonies within prior  $\beta$  grain at a lower cooling rate. These colonies basically consist of  $\alpha$  laths separated by relatively small  $\beta$  phase. Nucleation and growth process is the mechanism behind the formation of these  $\alpha$  laths [22]. The  $\alpha$  lamellae nucleates at the  $\beta$  grain boundaries and grows as parallel laths with same crystallographic orientations. A martensitic structure is formed at a higher cooling rate by the process of diffusion-less transformation [23]. A complete disappearance of globular primary  $\alpha$  phase at the solution heat treatment temperature of 1060 °C followed by quenching and ageing is observed. The disappearance of globular primary  $\alpha$  phase indicates that the  $\beta$  transus temperature has reached. The thickness of the  $\alpha$  laths in the transformed  $\beta$  grain increases with the decrease in the cooling rate as shown in Figs. 2a–d and 3a–d. It is to be noted that the size and orientation of the lamellae change with the reduction in the cooling rate (Table 3). At a higher rate of cooling, the thickness of the  $\alpha$  lamellae is found to be fine with random orientation. This has also been reported by various researchers in their investigations of titanium alloys [24, 25]. The thickness and volume

fraction of grain boundary  $\alpha$  increase with the decrease in the rate of cooling. The grain boundary  $\alpha$  phase is almost nil in water-quenched specimen, whereas a discontinuous grain boundary  $\alpha$  phase is found in oil-quenched specimen. This indicates that a critical cooling rate exists for the formation of complete grain boundary  $\alpha$  phase which is also reported in some investigation of titanium alloys. The formation of the lamellae or plates becomes more coarser as the cooling rate decreases because the driving force for nucleation within the grains is reduced. The size of the colony increases with the decrease in the cooling rate at a particular solution heat treatment temperature. In case of small transformed  $\beta$  grain size, the cluster of  $\alpha$  lamellae originates at the grain boundary of transformed  $\beta$  grain and occupies the whole grain maintaining the similar crystallographic orientation at a lower cooling rate. However, the transformed  $\beta$  grain size reduces with the decrease in the cooling rate and the colonies terminate after a certain distance beyond which basket-weave structure dominates.

#### 3.2 Hardness

Table 4 shows the variation of bulk hardness with the cooling/quenching media. An increment in the hardness has been observed as the cooling rate was increased. This is

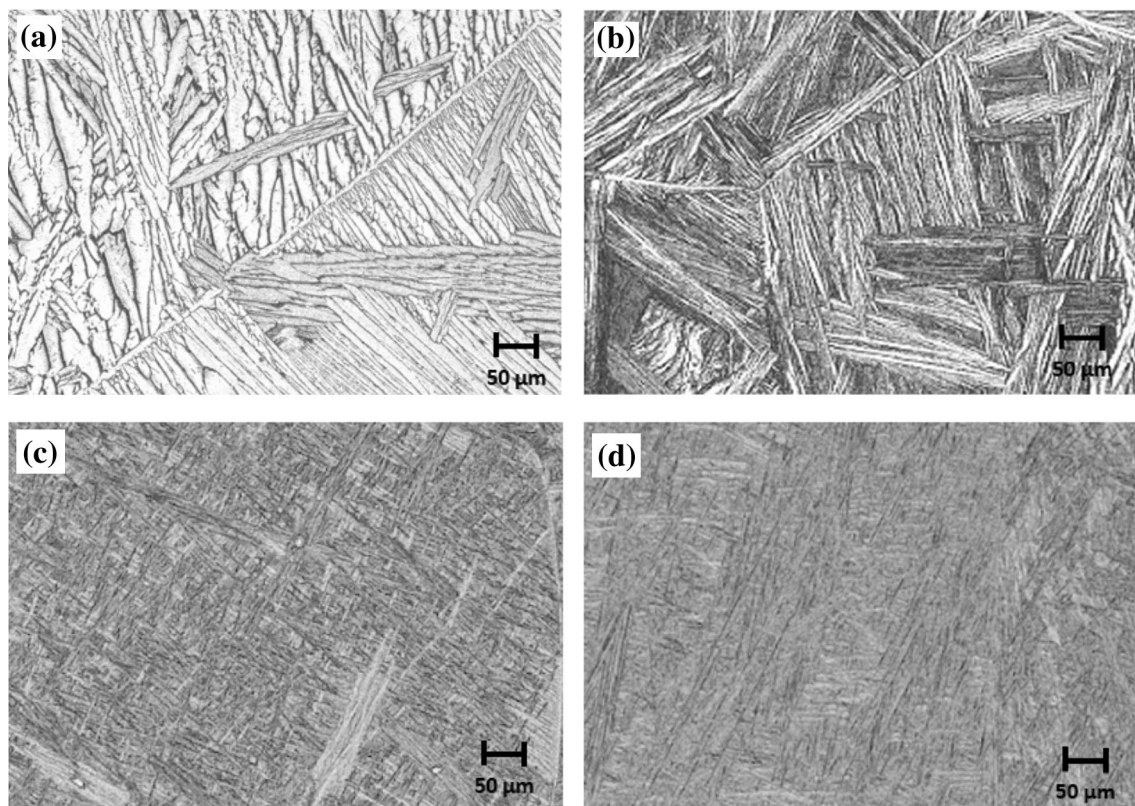


**Fig. 2** Optical micrograph at a magnification of 1000X: **a** furnace-cooled, **b** air-cooled, **c** oil-quenched, **d** water-quenched

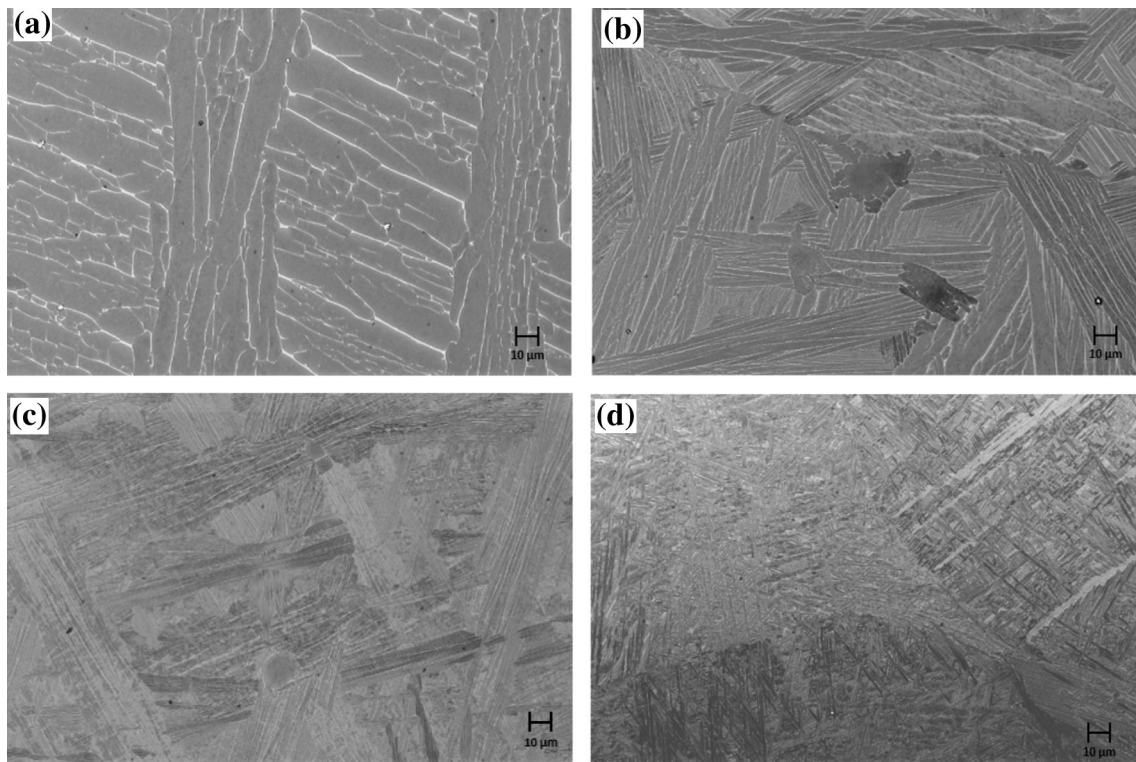


**Fig. 3** SEM micrograph: **a** furnace-cooled, **b** air-cooled, **c** oil-quenched, **d** water-quenched

**Table 3** Average  $\alpha$  lamellae thickness distribution with the quenching media

Cooling/quenching media	$\alpha$ lamellae thickness ( $\mu\text{m}$ )—average and standard deviation
FC	$9.40 \pm 0.48$
AC	$3.77 \pm 0.46$
OQ	$1.45 \pm 0.31$
WQ	$0.77 \pm 0.18$

**Table 4** Variation of hardness with the quenching medium

Cooling/quenching medium	Hardness (Hv)—average and standard deviation
FC	$320 \pm 1.96$
AC	$351 \pm 11.8$
OQ	$364 \pm 6.17$
WQ	$379 \pm 6.27$

due to the fact that the basket-weave microstructure increases the dislocation density at a higher cooling rate.

### 3.3 High-Cycle Fatigue (HCF)

In the present study, variation of fatigue life has been observed w.r.t. cooling rate at a stress level of 650 MPa as

shown in Fig. 4. It is noted that the fatigue life is minimum for the furnace-cooled condition and maximum for the water-quenched condition. The logarithmic S–N behaviour is completely linear as shown in Fig. 5 at all cooling rate conditions, as expected for most of the engineering alloys. A decrease in the fatigue life is also observed with the increase in the stress amplitude.

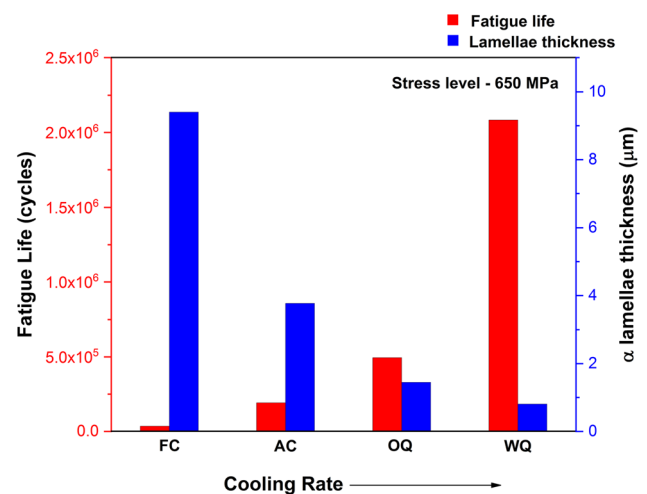


**Fig. 4** Variation of fatigue life and  $\alpha$  lamellae thickness with the cooling rate

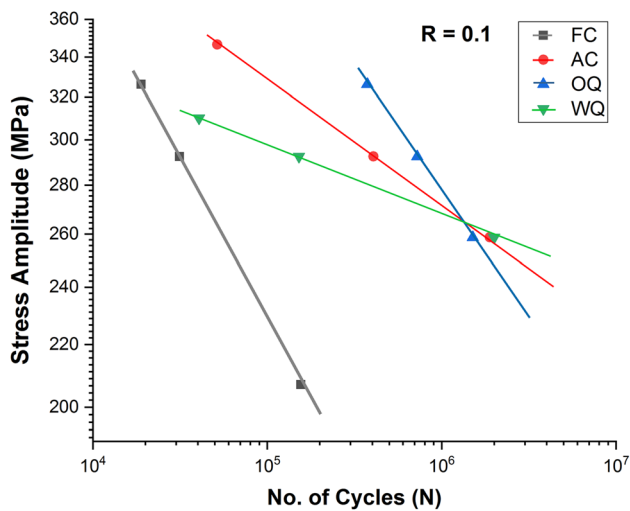


**Fig. 5** Stress-life plot on log–log scale

### 3.4 Fatigue Micro-mechanism

The high-cycle fatigue (HCF) strength depends upon the maximum length of the dislocation slip in the

**Table 5** Variation of fatigue strength coefficients and exponents for different cooling/quenching media

Cooling/ quenching media	Fatigue strength coefficient ( $\sigma_f$ ) (MPa)	Fatigue strength exponent ( $b$ )
FC	2276	– 0.19
AC	889	– 0.09
OQ	1917	– 0.14
WQ	1386	– 0.11

microstructure, and it increases with the reduction in the maximum dislocation slip length [25]. Irreversible slip present within the longest crystallographic slip band is found to be the main reason behind the crack nucleation [26, 27] during HCF. For the present study, it can be inferred that martensitic  $\alpha$  microstructure at higher cooling rate has reduced effective slip lengths. Microstructures at higher cooling rate tend to hinder the easy propagation of small surface nucleated cracks due to higher density of grain boundaries as well as because the  $\alpha$  laths act as the obstacle in the propagation of cracks [28, 29]. These reasons tend to slow down the crack growth rate and may have

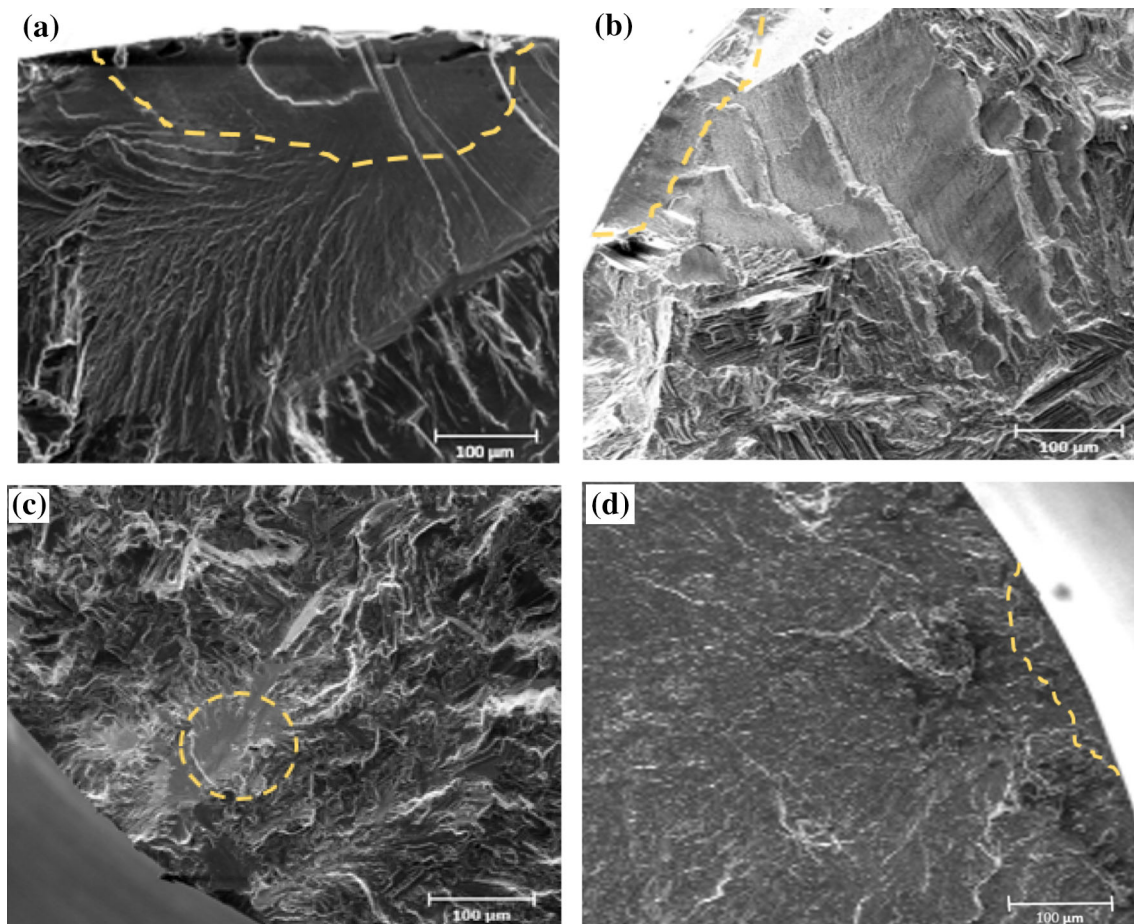


**Fig. 6** SEM micrograph of the fractured specimen: **a** furnace-cooled, **b** air-cooled, **c** oil-quenched, **d** water-quenched

resulted in higher HCF strength as compared to samples with coarse lamellar microstructure. Coarse lamellar microstructure possesses  $\alpha$  structure aligned in the colonies with extended slip bands along the alignment. These larger slip bands provide less hindrance in propagation of cracks. Also, surface-initiated cracks prefer to propagate along the alignment of  $\alpha$  laths. Hence, the crack propagates faster along the planar slip bands in coarser lamellar microstructures and results in lower HCF strength. Surface hardness also affects the fatigue life. Most of the cracks initiate from the surface or subsurface region [30, 31]. Surface hardness resists the crack initiation at the surface. Hence, the higher the surface hardness, the lower will be the crack growth rate and higher fatigue life [32, 33].

Fractured specimens were examined under SEM to identify the crack initiation locations as well as the fracture features under the HCF loading. Fracture surface has two distinct zones, i.e. crack initiation zone and the fast fracture zone. Location of crack initiation can be easily identified within the crack initiation zone. It has been observed that the crack initiates mainly from the surfaces as shown in Fig. 6. The fraction of initiation sites is more in case of

furnace-cooled condition and decreases as the rate of cooling is increased. The higher the number of initiation zones, the lesser the fatigue life. These crack initiation facets have the plane surfaces. The fatigue fracture facets are known to have the near-basal orientation at the crack initiation sites. The occurrence of the faceted initiation sites under fatigue test condition is well explained by the Stroh model [34]. The stress component normal to the plane of crack has been studied for the formation and propagation of cracks. Stroh on the basis of his study proposed that the formation and propagation take place on the plane of maximum tensile normal stress.

### 3.5 Stress-Life Model

Stress-life relationship has been modelled by using Basquin's power law [refer Eq. (1)] which basically correlates the stress amplitude and the number of cycle reversals to failure [35]. A linear relationship is commonly observed between the logarithmic of the stress amplitude and the logarithmic of number of reversals of failure.

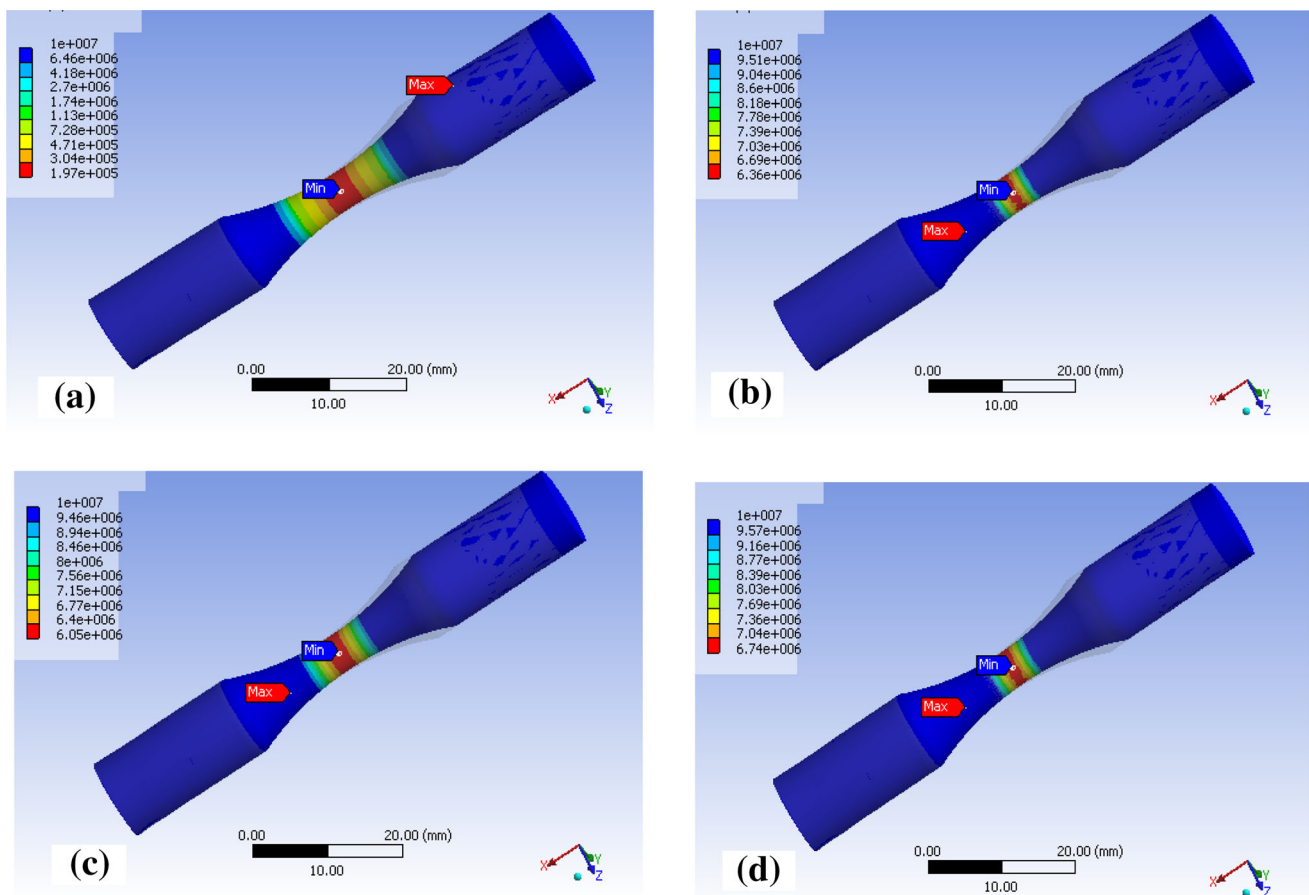


**Fig. 7** Fatigue life distribution of HCF sample: **a** furnace-cooled, **b** air-cooled, **c** oil-quenched, **d** water-quenched

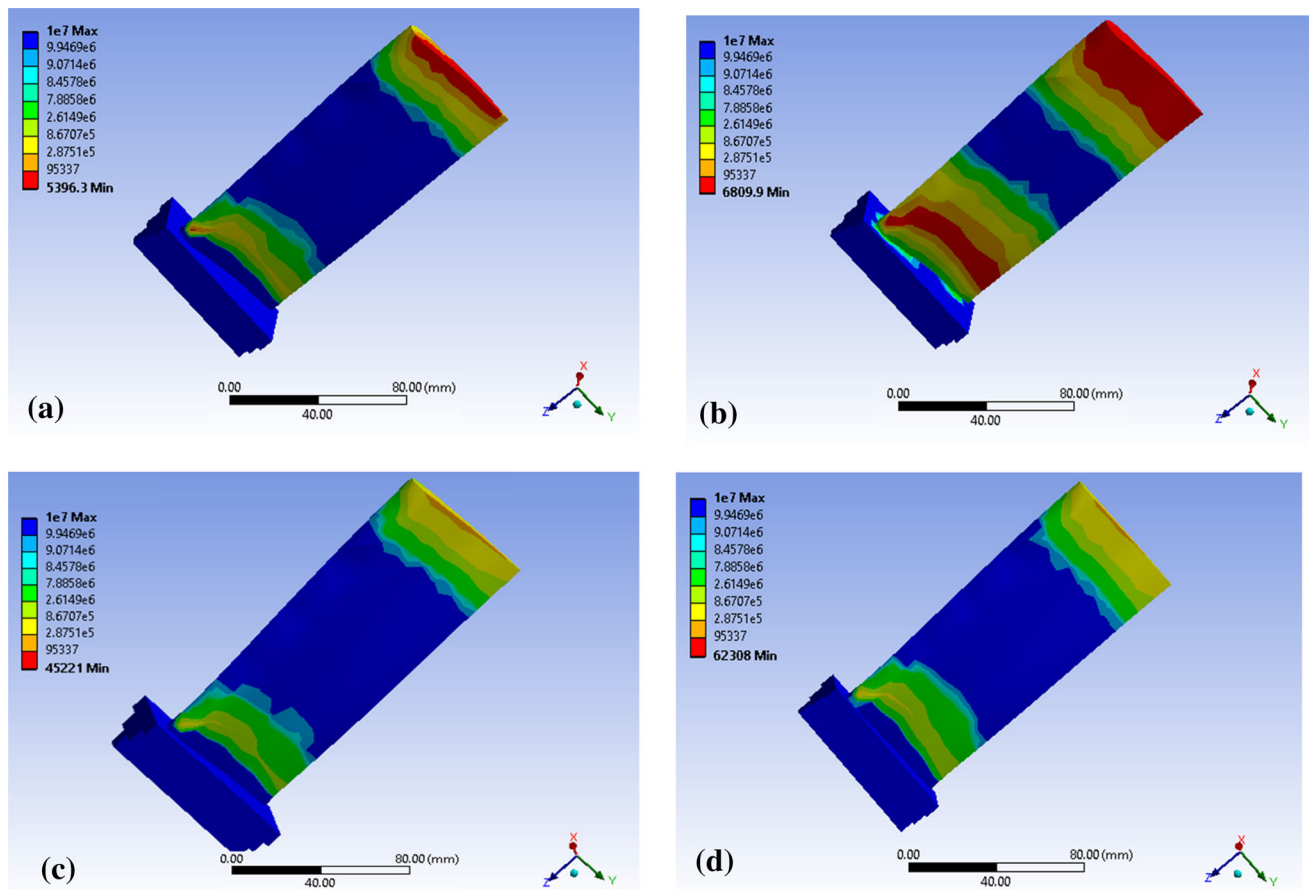


**Fig. 8** Fatigue life distribution of representative compressor blade: **a** furnace-cooled, **b** air-cooled, **c** oil-quenched, **d** water-quenched

$$\sigma_a = \frac{\Delta\sigma}{2} = \sigma_f (2N_f)^b. \quad (1)$$

$\sigma_f$  is the fatigue strength coefficient that indicates the true fatigue strength of the component and  $b$  is the fatigue strength exponent that indicates the slope of the material curve. Based on the fatigue test results, the master Basquin's equation has been deduced using MATLAB ("Appendix") which would predict the fatigue life of a component for any loading conditions in terms of mean stress for particular heat treatment conditions.

The values of fatigue strength coefficients and exponents for different cooling/quenching media are given in Table 5. In the present study, the fatigue strength coefficient ( $\sigma_f$ ) varies from 889 to 2276 MPa that represents the true fatigue strength at a particular heat treatment condition.

The fatigue strength exponent varies from -0.09 to -0.187 depending upon the cooling rate. The value of  $b$  obtained for this alloy is similar as observed for most of the alloys ( $b = -0.05$  to  $-2.0$ ) [36–38]. Morrow et al. [39] proposed a relation between the fatigue strength exponent ( $b$ ) and cyclic strain hardening exponent ( $n'$ ) as follows:

$$b = \frac{-n'}{1 + 5n'}. \quad (2)$$

For typical IMI 834, the value of cyclic strain-hardening exponent  $n'$  has been reported to be  $\sim 0.18$  at room temperature [40]. The theoretical value of fatigue strength exponent ( $\sim -0.1$ ) as given by Eq. (2) is within the range of the experimental value ( $-0.09$  to  $-0.19$ ).

### 3.6 Finite Element Modelling and Simulation

ANSYS Workbench 19.0 has been used in order to simulate the life and behaviour of specimens as well as the components under the action of cyclic loading. Furthermore, fatigue module of ANSYS Workbench has been selected that basically uses stress-life or strain-life model for the analysis. The stress-life model thus obtained from the experimental data has been implemented and integrated with the finite element analysis to develop a fatigue model. The fatigue life distribution on the basis of fatigue model that is generated incorporating the stress-life model is shown in Fig. 7.



The generated fatigue model was further extended for the aero-engine components as shown in Fig. 8. Solid elements having three degrees of freedom at each node has been used for the analysis. Furthermore, a tetrahedral mesh size of 0.5 mm has been used. Mesh has been further refined at the top surface as well as near to the fir-tree joint. A rotational velocity of 4000 RPM was applied for each cooling/quenching medium. A frictionless support was used at the top surface, and the fir-tree joint at the bottom was fixed. A significant variation in the fatigue life of IMI 834 at different cooling/quenching media has been observed.

Generally, aero-engine components are subjected to complex monotonic and cyclic loadings and it should sustain the complex loading throughout its life span without premature failure. This could be done by imparting the desired and required property at various sections of the components as per the loading conditions. Furthermore, these properties can be achieved by tailoring the microstructure. Hence, sectional heat treatment could be done to generate different microstructures in the same aero-engine components as per the desired and required uniaxial and cyclic properties at different sections. The present experimental and simulation studies suggest that the microstructures can be tailored through different heat treatments to achieve the desired cyclic properties.

#### 4 Conclusions

Based on the microstructural and high-cycle fatigue study of near- $\alpha$  titanium alloy IMI 834, the following can be concluded:

- A wide range of microstructure is generated by varying the heat treatment conditions. With the decrease in the

cooling rate, the  $\alpha$  lamellae thickness increases. Complete disappearance of globular  $\alpha$  occurs at a solution heat treatment temperature of 1060 °C.

- The fatigue life of IMI 834 increases with the increase in the cooling rate at a particular stress level. Fractographs reveal that the crack initiation zones have flat surfaces and have near-basal orientations.
- Basquin's equation has been deduced for a particular heat treatment condition, and Basquin's parameters have been evaluated. The parameters are found within the limit of titanium alloy as per the literature. The stress-life model based on experimental data at specimen level is integrated with finite element analysis to develop the fatigue model. The fatigue model thus obtained is extended to aero-engine components to study the elemental fatigue life corresponding to cyclic loading.

**Acknowledgements** The constant support and encouragement from Dr. G. Madhusudan Reddy, Director and Dr. T. K. Nandy, Associate Director, DMRL, is gratefully acknowledged. Technical discussions on Ti alloys with Dr. S. Banumathy, DMRL, are also acknowledged. Mr. S. Ahmad, DMRL and his team is acknowledged for timely availability of fatigue specimens for testing. Thanks are also due to Dr. Vikas Kumar (Former Director, DMRL) and Dr. D.V.V. Satyanarayana, Sc 'G', Head, Mechanical Behaviour Group, DMRL, for their guidance and support in executing this study. The authors would also like to thank DRDO, India, for funding this research.

#### Appendix: MATLAB Code

```

%*****%
% MATLAB code to evaluate fatigue strength coefficient and exponent
%*****%

clc;                % clears command window
closeall;          % deletes all figures whose handles are not hidden.
clearall;         % clear/delete the variables created in Workspace.
% Input stress range( $\Delta\sigma = \sigma_{max} - \sigma_{min}$ ) from the user.
y=input('Input stress range (in MPa) : ');
% Input number of cycles(N) from the user.
x=input('Input corresponding number of cycles: ');
% Basquin's equation:  $\sigma_a = (\Delta\sigma/2) = \sigma_f \cdot (2N)^b$ 
%  $\sigma_a$  -Stress amplitude,  $\Delta\sigma$ -stress range,  $\sigma_f$  -fatigue strength coefficient
% N-number of cycles, b- fatigue strength exponent
Y=0.5*y;          % Stress amplitude = 0.5* stress range i.e.  $\sigma_a = (\Delta\sigma/2)$ 
X=2*x;           % 2* number of cycles i.e. 2N
disp(Y);          % Displays stress amplitude  $\sigma_a = (\Delta\sigma/2)$ 
disp(X);          % Displays 2N
%Plotting the data for  $\Delta\sigma / 2$  vs 2N
plot(X,Y,'+r');
hold on;
% Polynomial curve fitting of log data values
% We have linear equation
% Simplifying:  $\log(Y) = \log(a \cdot X.^b) = \log a + b \cdot \log(X)$ 
p=polyfit(log(X),log(Y),1);
% Evaluating fatigue strength coefficient and exponent
b=p(1);
a=exp(p(2));      % Accounting for the log transformation
fprintf('Fatigue strength coefficient = %d MPa',a);
fprintf('\nFatigue strength exponent = %d ',b);
Xp=X(end):1:X(1);
Yp=a*Xp.^b;
%Final plot
plot(X,Y,'+r',Xp,Yp);

%*****%

```

## References

- [1] Lütjering G, Williams J C, and Gysler A, in *Microstructure and Properties of Materials* (2000), vol. 2, pp. 1–77.
- [2] Bania P J, Hutt A J, and Adams R E, in *Beta Titanium Alloys in the 1990's* (1993).
- [3] Welsch G, Boyer R, and Collings E W (eds) *Materials Properties Handbook: Titanium Alloys*, ASM International, Cleveland (1993).
- [4] Cowles B A, *Int J Fract* **80** (1996) 147.
- [5] Peters M, Lütjering G, and Ziegler G, *Zeitschrift für Metallkunde* **74** (1983), 274.
- [6] Du Z, Xiao S, Xu L, Tian J, Kong F, and Chen Y, *Mater Des* **55** (2014) 183.
- [7] Neal D F, in *Titanium Science and Technology*, (eds) Lütjering G, Zwicker U, and Ansd Bunk W, DGM, Oberursel Germany (1985), vol. 4, pp. 2419–2424.
- [8] Sha W, and Malinov S, *Titanium Alloys: Modelling of Microstructure, Properties and Applications*, Elsevier, Amsterdam (2009).
- [9] Wu G Q, Shi C L, Sha W, Sha A X, and Jiang H R, *Mater Des* **46** (2013) 668.
- [10] Ivanova S G, Biederman R R, and Sisson R D, *J Mater Eng Perform* **11** (2002) 226.
- [11] Zuo J H, Wang Z G, and Han E H, *Mater Sci Eng A* **473** (2008) pp.147.
- [12] Lütjering G, and Williams J C, *Titanium*. Springer, Berlin (2007).

- [13] Wagner L and Lütjering G, in *Titanium*, Science and Technology, Les Editions de Physique (1988) p. 345.
- [14] Ivanova S G, Cohen F S, Biederman R R, and Sisson Jr R D, *Role of Microstructure in the Mean Stress Dependence of Fatigue Strength in Ti–6Al–4V alloy*, Worcester Polytechnic Institute, Worcester (1999).
- [15] Peters M, Gysler A, Lütjering G. in *Titanium'80 Science and Technology* (eds Kimura H and Izumi O, AIME, New York (1980), pp. 1777–1786.
- [16] Wu Z, Kou H, Tang L, Chen W, Han X, Deng Y, Tang B, and Li J, *Eng Fract Mech* **235** (2020) 107129.
- [17] Singh N, and Singh V, *Mater Sci Eng A* **325** (2002) 324.
- [18] Hardt S, Maier HJ, and Christ HJ, *Int J Fatigue* **21** (1999) 779.
- [19] Golden P J, John R, and Porter III W J, *Procedia Eng* **2** (2010) 1839.
- [20] Furuya Y, and Takeuchi E, *Mater Sci Eng A* **598** (2014) 135.
- [21] Neal D F, and Blenkinsop P A, *Acta Metallurgica* **24** (1976) 59.
- [22] Ramanujan R V, and Maziasz P J, *Metall Mater Trans A* **27** (1996) 1661.
- [23] Bywater K A, and Christian J W, *Philos Mag* **25** (1972) 1249.
- [24] Balasundar I, Raghu T, and Kashyap B P, *Mater Perform Charact* **8** (2019) 932.
- [25] Semiatin S L, *Metall Mater Trans A* (2020) 1–33.
- [26] Lucas J J, in *Titanium Science and Technology* (eds Jaffee R I and Burte H M, Plenum Press, New York, NY (1973), vol. 3, pp. 2081–2095.
- [27] Nalla R K, Ritchie R O, Boyce B L, Campbell J P, and Peters J O, *Metall Mater Trans A* **33** (2002) 899.
- [28] Brown C W, and Hicks M A, *Fatigue Fract Eng Mater Struct* **6** (1983) 67.
- [29] Wang Q Y, Bathias C, Kawagoishi N, and Chen Q, *Int J Fatigue* **24** (2002) 1269.
- [30] Xue H, Gao T, Sun Z, and Zhang X, in *MATEC Web of Conferences*, EDP Sciences (2018), vol. 165, p. 20003.
- [31] Yadav V K, Gaur V, and Singh I V, *Mater Sci Eng A* **779** (2020) 139116.
- [32] Kondo Y, Sakae C, Kubota M, and Kudou T, *Fatigue Fract Eng Mater Struct* **26** (2003) 675.
- [33] Peters J O, and Lütjering G, *Metall Mater Trans A* **32** (2001) 2805.
- [34] Sinha V, Mills M J, Williams J C, and Spowart J E, *Metall Mater Trans A*, **37** (2006) 1507.
- [35] Basquin O H, in *Proc Am Soc Test Mater* (1910), vol. 10, pp. 625–630.
- [36] Stephens R I, Fatemi A, Stephens R R, and Fuchs H O, *Metal Fatigue in Engineering*, Wiley, New York (2001).
- [37] Ellyin F, in *Fatigue Damage, Crack Growth and Life Prediction*. Springer, Dordrecht (1997), pp. 145–178.
- [38] Meyers M A, and Chawla K K, *Mechanical Behavior of Materials*, Cambridge University Press, Cambridge (2008).
- [39] Morrow J, in *Internal Friction, Damping, and Cyclic Plasticity*. ASTM International (1965).
- [40] Naglakshmi G, and Kumar V, High temperature fatigue crack growth behavior of IMI 834 Ti alloy, DMRL Technical Report No. 371 (2005).

**Publisher's Note** Springer Nature remains neutral with regard to jurisdictional claims in published maps and institutional affiliations.